


RESEARCH ARTICLE

Interpenetrated Three-Dimensional Covalent Organic Framework for Selective Adsorption of C₂H₂ Over CO₂ and C₂H₄

Sayan Maiti¹ | Kui Tan¹ | Shubo Geng² | Amit Kumar Gupta¹ | Peter E. VanNatta¹ | Daqiang Yuan³ | Zhenjie Zhang² | Gaurav Verma¹ | Thamraa AlShahrani⁴ | Shengqian Ma¹ 

¹Department of Chemistry, University of North Texas, Denton, Texas, USA | ²College of Chemistry, Key Laboratory of Advanced Energy Material Chemistry (Ministry of Education), Nankai University, Tianjin, China | ³Fujian Institute of Research on the Structure of Matter, Chinese Academy of Sciences, Fuzhou, China | ⁴Department of Physics, College of Science, Princess Nourah bint Abdulrahman University, Riyadh, Saudi Arabia

Correspondence: Shengqian Ma (Shengqian.Ma@unt.edu)

Received: 7 April 2025 | **Revised:** 23 May 2025

Funding: The authors acknowledge the financial support from the Robert A. Welch Foundation (B-0027) for this work. Partial support from Princess Nourah Bint Abdulrahman University Researchers Supporting Project number (PNURSP2025R1), Riyadh, Saudi Arabia (T.A.) is also acknowledged.

Keywords: dynamic breakthrough | gas separation | in situ FTIR | three dimensional COFs

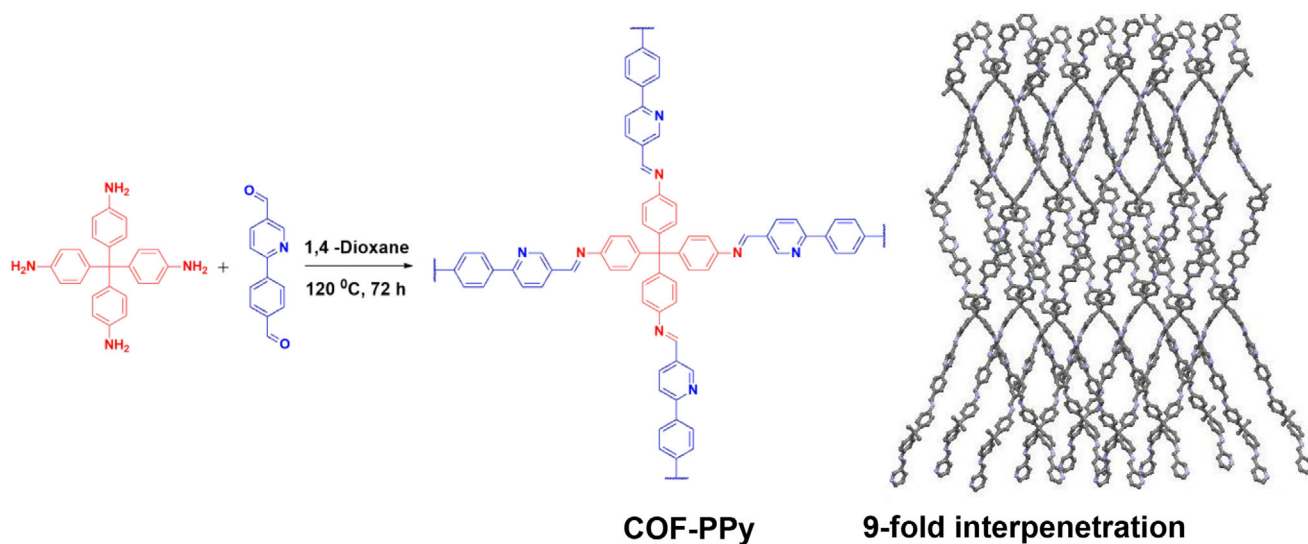
ABSTRACT

Selective separation of acetylene (C₂H₂) from carbon dioxide (CO₂) and ethylene (C₂H₄) mixtures is critical in the petrochemical industry due to their similar size and physicochemical properties. Developing three-dimensional porous covalent organic frameworks (3D COFs) remains challenging in this context. In this work, a non-symmetrical 2-phenyl pyridine based three-dimensional covalent organic framework (**COF-PPy**) has been synthesized, which features a rare dia-C9 fold interpenetrated structure as suggested by computational simulations. **COF-PPy** exhibits high acetylene (C₂H₂) adsorption capacity (4.5 mmol g⁻¹ at 298 K), as well as excellent separation and purification performance for C₂H₂/CO₂ and C₂H₂/C₂H₄ mixtures. The *in situ*-FTIR studies suggest that the multi-point interactions between nitrogen centers of **COF-PPy** and H-C≡CH (COF-Pyridine-N...H-C≡C-H and COF-imine-N...H-C≡CH) account for the higher affinities for C₂H₂ over other gases. Furthermore, dynamic breakthrough studies reveal that **COF-PPy** can be employed as an effective adsorbent for the efficient separation of C₂H₂ from CO₂ and C₂H₄. In addition, **COF-PPy** exhibits lower heat of adsorption (Q_{st}) values with high adsorption capacity for C₂H₂ as compared to previously reported C₂H₂-selective adsorbents, indicating less regeneration energy. Our work therefore provides some new avenues for the design and construction of 3D COFs for efficient C₂H₂ capture and separation.

1 | Introduction

As an emerging class of crystalline nanoporous materials, covalent organic frameworks (COFs) have garnered a lot of interest because of their high surface areas, customizable constructions, and adaptability to a wide range of uses, including gas storage, catalysis, molecule separation, and sensing [1–3]. COFs offer attractive solutions for potential applications due to their inher-

ent designability through the selection of building blocks and functional groups [4, 5]. However, despite these advantages, most COFs feature two-dimensional (2D) structures with difficulty in pore size control to micropore and ultra-micropore thus limiting their effectiveness in gas separation applications [6, 7]. The development of three-dimensional (3D) interpenetrated COFs, which could overcome many of the structural drawbacks of non-interpenetrated 2D COFs, has been a significant advancement in



SCHEME 1 | Synthetic scheme of COF-PPy.

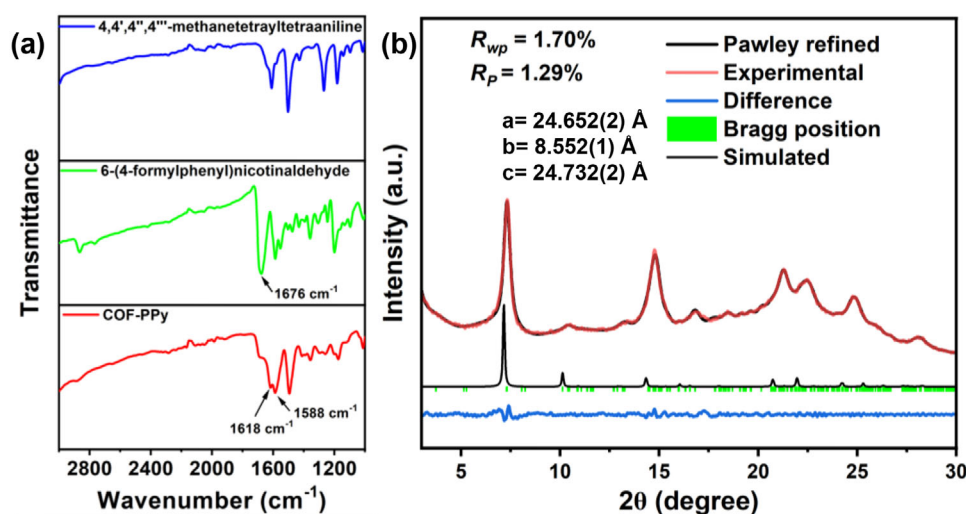


FIGURE 1 | a) FT-IR, and b) PXRD of COF-PPy.

the field [8–11]. In COFs, interpenetration is the process by which two or more networks of the framework structures spatially interconnect between the layers with one another to build a stronger, more stable network with reduced pore size beneficial for separation applications, specially the separation of acetylene (C_2H_2) from other C_2 hydrocarbon gases (ethylene (C_2H_4), ethane (C_2H_6)) and carbon dioxide (CO_2) gas mixtures [9, 10].

It is well known that high purity is required for C_2H_2 which is among the most used organic raw materials for synthetic industrial compounds, particularly 1,4-butyne diol and derivatives of acrylic acid. C_2H_2 typically occurs as a by-product of the combustion of hydrocarbons, along with C_2H_4 and CO_2 [12]. On the other hand, removing C_2H_2 contamination from C_2H_4 is also important in the petrochemical industry since C_2H_2 is poisonous to the C_2H_4 polymerization catalyst used in polyethylene manufacturing, resulting in significantly lower-quality polyethylene [13]. However, it is a challenging task to separate C_2H_2 from $\text{C}_2\text{H}_2/\text{C}_2\text{H}_4$ and $\text{C}_2\text{H}_2/\text{CO}_2$ mixtures due to their similar molecular shape, kinetic diameter, boiling temperatures, and

electronegativity. The techniques most commonly employed for removing C_2H_2 typically involve liquid absorbent materials or cryogenic distillation, which are cost- and energy-intensive [14]. On the other hand, alternative methods such as membrane separation or adsorption offer substitutes with relatively lower energy costs. Recently, porous materials have gained widespread attention for $\text{C}_2\text{H}_2/\text{CO}_2$ and $\text{C}_2\text{H}_2/\text{C}_2\text{H}_4$ separations, with metal-organic frameworks (MOFs) leading the front. However, despite their high porosities and good separation performances, they suffer from the disadvantages of stability and cyclability over long periods of time [14]. COFs on the other hand can provide superior stability for continuous operation but remain relatively less explored owing to the difficulty in pore size control for sieving applications. For example, Wang and colleagues developed a pyridine-based 5-fold interpenetrated 3D COF that showed superior one-step C_2H_4 purification over a mixture of C_2H_6 and C_2H_4 [15]. This performance behavior was attributed to the $-\text{CH}\cdots\text{N}$ interactions between C_2H_6 and pyridine groups of the COF linkers. Another two-dimensional covalent organic framework based on boronic ester linkages was reported for effective capture

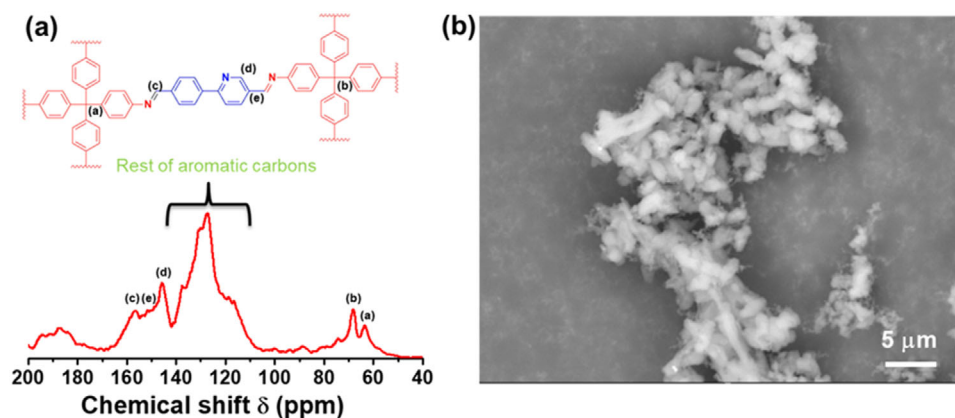


FIGURE 2 | (a) Solid-state ^{13}C NMR, and (b) SEM image of COF-PPy.

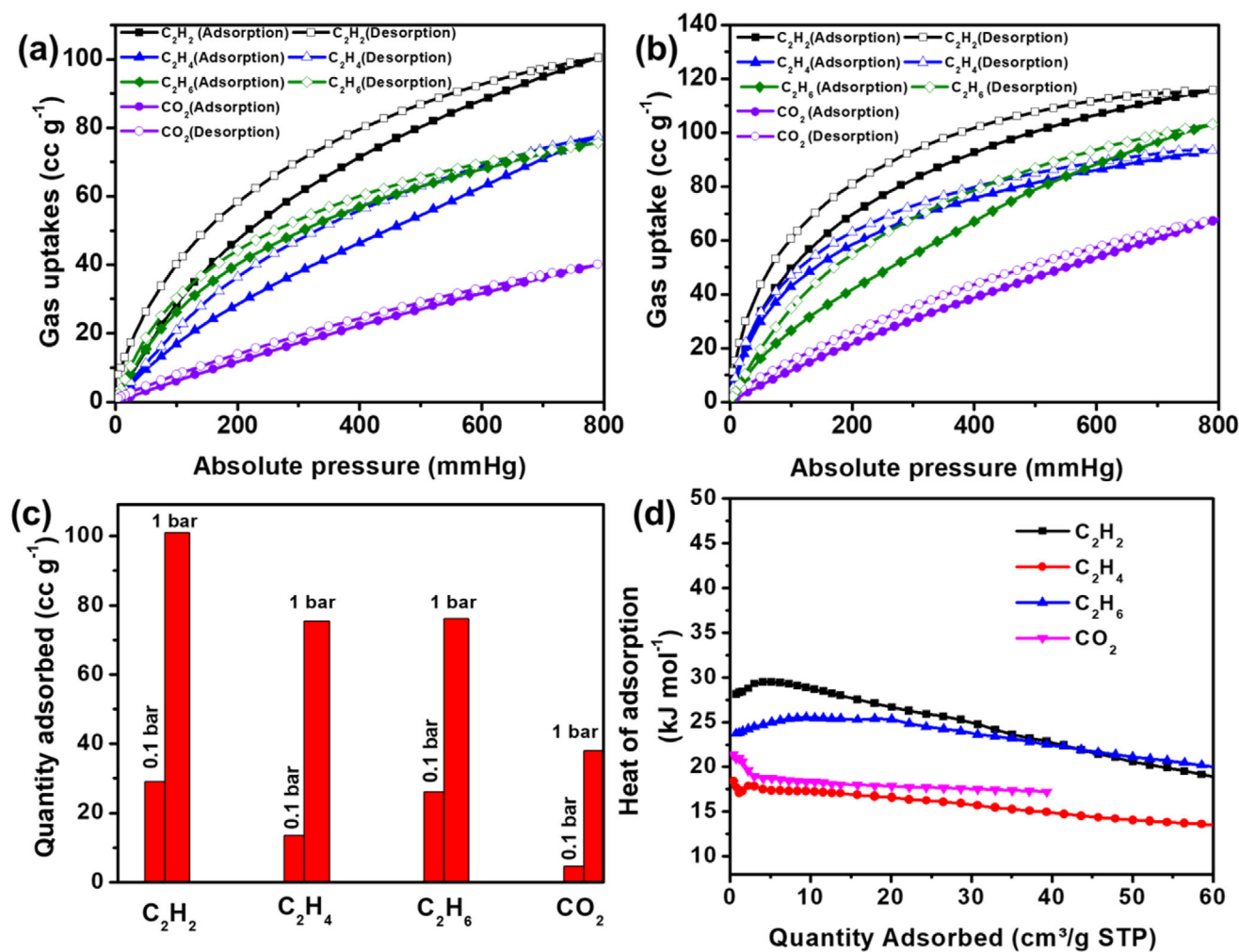


FIGURE 3 | a) Single-component C₂H₂, C₂H₄, C₂H₆, and CO₂ adsorption (filled symbols) and desorption (open symbols) isotherms of COF-PPy at (a) 298 K and (b) 273 K. (c) Comparison of 298 K adsorption capacities of the four gases for COF-PPy at 0.1 and 1 bar. (d) Q_{st} plots of C₂H₂, C₂H₄, C₂H₆ and CO₂ for COF-PPy.

of C₂H₂ over CO₂ via the $\pi \cdots \pi$ interactions between C \equiv C and the aromatic rings of COF [16]. Sun *et al.* utilized a cobalt-unctionalized two-dimensional covalent organic frameworks for efficient C₂H₂/CO₂ separation via strong host-guest interactions [17]. Zhu *et al.* developed a system of two-dimensional crystalline

polyimide porous organic framework for selective adsorption of C₂H₂ over C₂H₄, and the separation performance was attributed to the strong H-bonding between the HC \equiv CH and O atoms in the COF backbone [3]. Our group also recently published work on single-molecule trapping for selective capture of C₂H₂ from

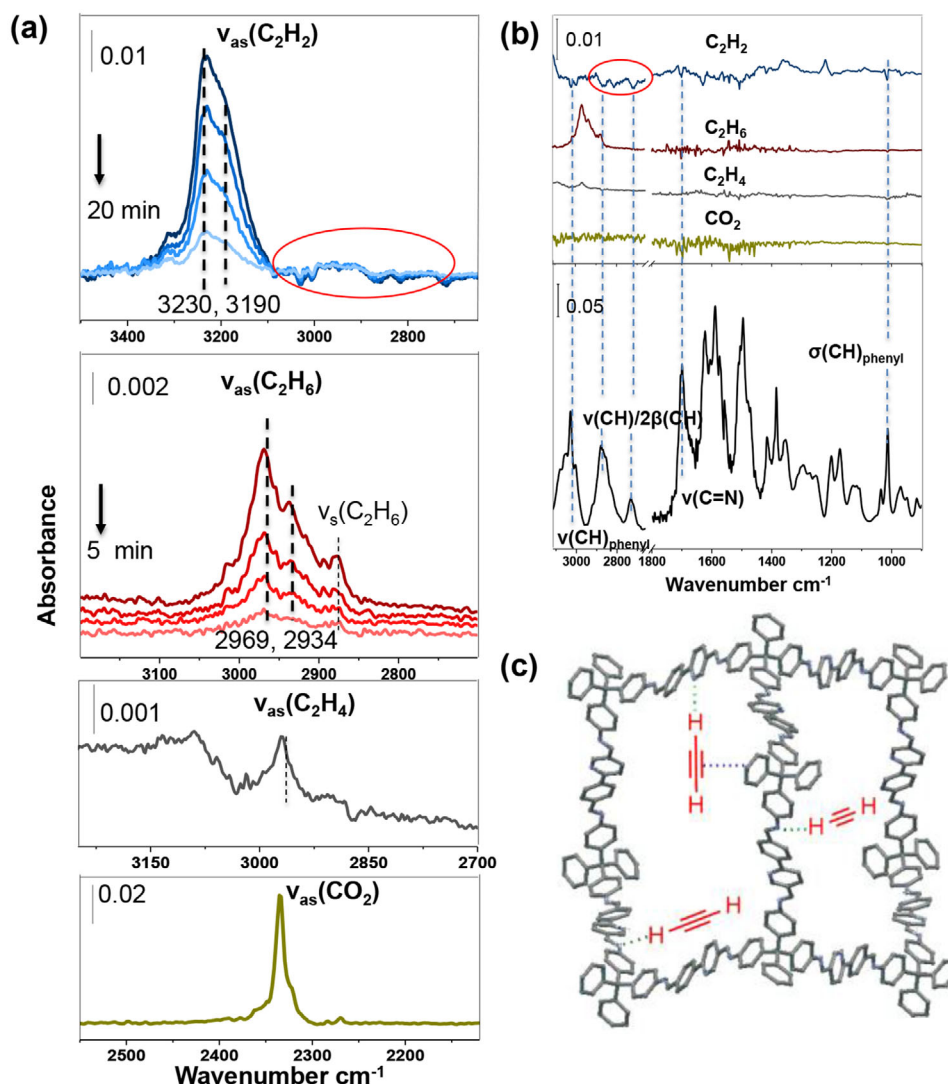


FIGURE 4 | (a) IR spectra showing the asymmetric stretching band of adsorbed C_2H_2 , C_2H_6 , C_2H_4 , and CO_2 inside COF upon loading C_2H_2 gas at ≈ 1 bar and 298 K. (b) Difference spectra showing the perturbation occurring to COF structure upon loading gases; each is referenced to the bottom spectrum of activated COF in vacuum. (Notation and acronym: ν , stretch; δ , deformation; β , bending; as, asymmetric; and s, symmetric). (c) Schematic representation of interactions between the $\text{H}-\text{C}\equiv\text{CH}$ and COF-PPy backbone.

C_2H_4 -rich gas mixtures using 2D-COFs [18]. Thus, it becomes imperative that for specific gas adsorption and separation from a broad spectrum of gas mixtures, it is essential to install selective groups or atoms and create interpenetrated 3D-COFs that can provide sieving behavior with suitable pores as well as resistance to external stresses and deformation.

This work describes the development of a microporous three-dimensional COF (**COF-PPy**) based on 2-phenyl pyridine and tetrahedrally symmetric 4,4',4'',4'''-methanetetrayltetraaniline as secondary building block units (Scheme 1). The topology of **COF-PPy** is a rare example of nine-fold interpenetrated *dia* networks among COFs. C_2H_2 is efficiently captured by **COF-PPy** compared to C_2H_4 , CO_2 , and C_2H_6 . Furthermore, dynamic breakthrough experiments showed that **3D-COF-PPy** can effectively purify C_2H_4 and CO_2 from mixtures of $\text{C}_2\text{H}_2/\text{C}_2\text{H}_4$ and $\text{C}_2\text{H}_2/\text{CO}_2$ in a single step. In situ-IR studies further supported detailed evidence on the impact of the mechanism of chemisorption and physisorption processes. This is explained by the fact that

COF-PPy's more accessible pores as well as the presence of pyridine and imine groups can improve the C_2H_2 -capture ability by interacting with C_2H_2 to generate strong $\text{C}-\text{H}\cdots\text{N}$ interactions. This performance is better than several other reported COFs and even at par with a few other benchmark porous materials.

2 | Results and Discussion

2.1 | Structural Characterization

The **COF-PPy** was obtained by heating a solution of 1,4-dioxane containing the non-symmetric 2-phenyl pyridine and the tetrahedrally symmetric 4,4',4'',4'''-methanetetrayltetraaniline in 6 M aqueous acetic acid to 120 degrees for three days in a sealed tube followed by simple filtration and washing with anhydrous 1,4-dioxane and tetrahydrofuran (THF). The resultant material was immersed in tetrahydrofuran for three days and dried under vacuum to yield **COF-PPy** as a fine yellow powder in 77%

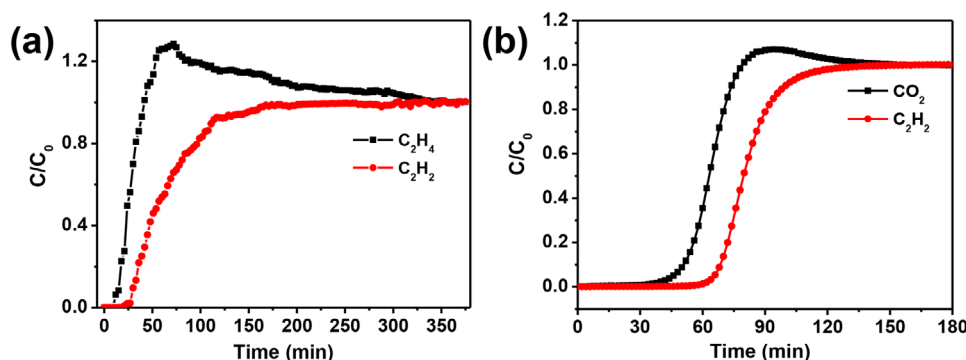


FIGURE 5 | (a) Dynamic breakthrough curves of C_2H_2/C_2H_4 ($v/v = 1:99$) mixture and (b) C_2H_2/CO_2 ($v/v = 1:1$) with a total flow rate of 1 mL min^{-1} .

yield. Several spectroscopic techniques were utilized to prove the successful construction of the 3D **COF-PPy**. FT-IR spectra of the **COF-PPy** show stretching bands at 1618 and 1588 cm^{-1} for imine ($-C=N-$) and aromatic $-C=C-$ bonds respectively, indicating the presence of imine linkages in **COF-PPy** [19]. The disappearance of aldehyde peaks of 2-phenyl pyridine moiety at $\sim 1676 \text{ cm}^{-1}$ in **COF-PPy** further established the formation of imine linkages in the framework (Figure 1a). **COF-PPy** shows several sharp PXRD peaks at 2θ values of 7.3 , 10.4 , 14.5 , 21 , 22.3 , and 24.6° , suggesting the formation of a highly crystalline framework structure (Figure 1b). The experimental PXRD pattern is in a good agreement with the PXRD pattern predicated from the computational simulation. Moreover, the simulations reveal that **COF-PPy** adopts *dia* C-9 folded interpenetration topology. Pawley refinement of the PXRD patterns using this model generated unit cell parameters of: $a = 24.652(2) \text{ \AA}$, $b = 8.552(1)$, and $c = 24.732(2) \text{ \AA}$ ($R_{wp} = 1.70\%$ and $R_p = 1.29\%$), with a good agreement between the experimental and simulated profiles.

^{13}C solid-state NMR measurements also demonstrate the formation of imine linkages and desired functionalities in **COF-PPy**. The peaks at 158 – 156 ppm suggest the presence of two types of imine bonds in the 3D framework structure due to the nonsymmetrical aldehyde building block unit (Figure 2a). Apart from that, two peaks also arise at 69 and 64 ppm due to two different types of aliphatic carbons attached to the $4,4',4'',4'''$ -methanetetrayltetraaniline unit in **COF-PPy**. The scanning electronic microscopy imaging further implies a uniform morphology with aggregates of small plate-shaped crystals of **COF-PPy** (Figure 2b). **COF-PPy** shows high thermal stability up to 450°C (Figure S3), after an initial loss of solvent from the pores.

2.2 | Surface Area Measurements

The permanent porosity, specific surface area, and pore size of the **COF-PPy** were evaluated by N_2 sorption isotherms at 77 K , which demonstrate that the COF exhibits type I isotherm indicating microporosity, with a BET surface area of $752 \text{ m}^2 \text{ g}^{-1}$ (Figure S2). The nonlocal density functional theory (NLDFT) model was used to calculate the pore size distribution of **COF-PPy**, and the results show that the average pore size is ≈ 0.8 – 1.1 nm . These characteristics establish the formation of **COF-PPy** with high structural regularity, architectural robustness, and intrinsic porosity.

2.3 | Low-Pressure Gas Adsorption Measurements

In order to assess their gas adsorption capacities, we investigated the single-component C_2H_2 , C_2H_4 , C_2H_6 , and CO_2 sorption isotherms of **COF-PPy** at 298 and 273 K (Figure 3a,b, respectively). The material shows the greatest affinity toward C_2H_2 over the other gases, with the uptake reaching $101 \text{ cm}^3 \text{ g}^{-1}$ at 298 K and 1 bar . As expected, the uptake increases to $116 \text{ cm}^3 \text{ g}^{-1}$ at 273 K (Figure 3c). The C_2H_2 adsorption capacity of **COF-PPy** at 298 K and 1 bar is significantly higher than that of other benchmark COFs (Table S1) such as NUS-71/72 (42.4 and $48 \text{ cm}^3 \text{ g}^{-1}$) [16], PAF-110 ($49.95 \text{ cm}^3 \text{ g}^{-1}$) [3], PAF-120 ($50.85 \text{ cm}^3 \text{ g}^{-1}$) [20], UPC-COF-1 ($89.8 \text{ cm}^3 \text{ g}^{-1}$) [17], Py-Na COF ($38 \text{ cm}^3 \text{ g}^{-1}$) [21] and HOF-FJU-100a ($\approx 40 \text{ cm}^3 \text{ g}^{-1}$) [22]. Furthermore, under comparable circumstances, these values exceed some forefront MOFs such as CAU-10-H ($89.8 \text{ cm}^3 \text{ g}^{-1}$), FJU-112a ($74 \text{ cm}^3 \text{ g}^{-1}$), UTSA-300 ($68.9 \text{ cm}^3 \text{ g}^{-1}$), and NKMOF-1-Ni ($61 \text{ cm}^3 \text{ g}^{-1}$) [23–25]. Significant interactions between 3D-**COF-PPy** and C_2H_2 are indicated by the C_2H_2 uptake capacities of **COF-PPy** in the ultralow (0.01 bar) and low pressure (0.1 bar) regimes, which are 3.1 and $23 \text{ cm}^3 \text{ g}^{-1}$ at 298 K , and increase to 8.5 and $43 \text{ cm}^3 \text{ g}^{-1}$ at 273 K , respectively. To the best of our knowledge, very few other COF adsorbents exhibit such large uptakes at ultralow pressures for C_2H_2 . In contrast, the uptakes of C_2H_4 , C_2H_6 , and CO_2 for **COF-PPy** are much lower with the corresponding values of 63 , 75 , and $50 \text{ cm}^3 \text{ g}^{-1}$ at 298 K and 1 bar , respectively. It is interesting to note that C_2H_2/CO_2 has the greatest uptake ratio of >2.6 as compared to C_2H_2/C_2H_4 and C_2H_2/C_2H_6 .

The gas adsorption performance of **COF-PPy** thus leads us to postulate that the addition of pyridine groups to the 3D networks greatly increases the C_2H_2 adsorption capacity through extra pyridine-acetylene interactions. To investigate further, the affinities of **COF-PPy** for all the gases were assessed using the Clausius-Clapeyron equation to calculate the coverage-dependent isosteric heat of adsorption (Q_{st}). For C_2H_2 , **COF-PPy** shows a Q_{st} of 28 kJ mol^{-1} at nearly zero loading, whereas for CO_2 it is much lower at 21 kJ mol^{-1} . C_2H_2 thus shows a stronger affinity than CO_2 due to its smaller size and strong interactions with the pyridyl groups, which enables it to pack more molecules quite effectively into the same space inside the 3D **COF-PPy**. The Q_{st} of C_2H_2 shows a decrease with increasing C_2H_2 uptake, suggesting that adsorption sites with higher interaction energy are initially occupied followed by those with lower interaction energy. On the other hand, C_2H_4 has a substantially lower heat of adsorption (18 kJ mol^{-1}), indicating weaker binding interactions

with COF. For C_2H_6 , the material shows a comparable Q_{st} value $\approx 24 \text{ kJ mol}^{-1}$. Moreover, Q_{st} values of C_2H_2 for **COF-PPy** are lower than several reported C_2H_2 -selective porous adsorbents [18, 19, 21–23], making the regeneration process more energy efficient.

To evaluate the stability of the material after adsorption measurements, FT-IR and PXRD measurements on COF-PPy were carried out. The results reveal no major changes in the framework structure when compared to pristine COF-PPy (Figure S4). Thus, the material can be reutilized for subsequent measurements after washing it with acetone and THF, and activated again.

2.4 | Mechanistic Studies Using In Situ IR

To gain a deeper understanding of the sorption mechanism and superior performance of COF toward adsorbing C_2H_2 , we conducted in situ infrared (IR) spectroscopy measurements on **COF-PPy** by separately loading C_2H_2 , C_2H_6 , C_2H_4 , and CO_2 , respectively at $\approx 1 \text{ bar}$ and 298 K . The spectroscopic results are presented in Figure 4. Given that the spectra of the gas phase are prohibitively high, that hinders direct observation of the adsorbed species. We thus evacuated the gas phase by pumping the cell and collected the spectra immediately after $\sim 5 \text{ sec}$ of evacuation, i.e., the pressure drops below 500 mTorr that showing negligible gas-phase IR absorption. As shown in Figure 4a, the adsorbed molecules can be readily characterized by their asymmetric stretching mode (ν_{as}) absorption.

Note that the symmetric stretching modes of C_2H_2 , C_2H_4 , and CO_2 are IR in-active. Interestingly, C_2H_2 and C_2H_6 show two clearly distinguished ν_{as} bands in contrast to C_2H_4 and CO_2 , which show only one band. This points to two types of C_2H_2 and C_2H_6 molecules absorbed within the COF structure that give rise to distinct IR absorption features [26, 27], whereas only one type of C_2H_4 , and CO_2 is present under the same conditions. We further examined the perturbations occurring to the vibrational bands of COF upon loading the four gases. Figure 4b shows that COF bands are most affected after loading C_2H_2 . As shown in the difference spectra of Figure 4b, the CH-stretching/CH-bending Fermi resonance from $HC = N$ linkage, denoted as $\nu(CH)/2\beta(CH)$, and $C = N$ stretch modes [28], are clearly perturbed, indicated by the derivative-like feature; C-H stretching and in-plane deformation from phenyl ring of aldehyde linker, sensitive to the chemical environment [29, 30], show slight decrease of intensities; in addition, stretching of pyridine C–N bond at 1200 cm^{-1} is also blue-shifted [31]. All these point to multi-point interaction of C_2H_2 with COF structure (Figure 4c).

2.5 | Dynamic Breakthrough Experiments

To better understand the actual separation performance of C_2H_2/C_2H_4 ($v/v = 1:99$) and C_2H_2/CO_2 ($v/v = 1:1$) mixtures (Figure 5a,b) by **COF-PPy**, dynamic breakthrough experiments [32–34] were carried out under ambient conditions at a flow rate of 1 mL min^{-1} (Figure 5a,b). The curve suggests a distinct separation between C_2H_2 and C_2H_4 , whereby the C_2H_4 first eluted from the column and reached saturation in 7 min, and then C_2H_2 broke through with a substantially longer retention period of 27 min, indicating the effective separation performance

of the **COF-PPy** for C_2H_2/C_2H_4 mixtures. The estimated C_2H_4 productivity in C_2H_2/C_2H_4 separation is 5 mL g^{-1} . For the C_2H_2/CO_2 separation using **COF-PPy**, the material shows an impressive separation curve whereby CO_2 is passed through the columns with a short retention period of 30 min, followed by C_2H_2 with a significantly longer retention time of 67 min. This indicates that **COF-PPy** has a good C_2H_2/CO_2 separation performance and an exceptional capacity for C_2H_2 adsorption over CO_2 .

3 | Conclusion

In conclusion, we have successfully designed and synthesized a pyridine functionalized microporous 9-fold interpenetrated 3D COF (**COF-PPy**) that shows effective one-step CO_2 and C_2H_4 purification ability from C_2H_2/CO_2 and C_2H_2/C_2H_4 mixtures. The rational design of 3D **COF-PPy** using non-symmetric 2-phenyl pyridine ligand exhibits significantly enhanced C_2H_2 adsorption capacity. Multiple interaction sites for C_2H_2 are provided by **COF-PPy**, which leads to an increase in affinity over the other gases. We have further conducted in situ FTIR and dynamic breakthrough studies to understand the mechanism and evaluate the practical separation performance. This paper provides a direction of synthesis of the higher fold of interpenetrated 3D COF, and high performance of CO_2 and C_2H_4 purification from C_2H_2 mixture with high adsorption capacity. Given the encouraging uses of 3D COFs in gas separation, our research opens the door for the further development of functionalized 3D COFs for the effective separation of industrially relevant gases.

Acknowledgements

The authors acknowledge the financial support from the Robert A. Welch Foundation (B-0027) for this work. Partial support from Princess Nourah bint Abdulrahman University Researchers Supporting Project number (PNURSP2025R1), Riyadh, Saudi Arabia (T.A.) is also acknowledged.

Conflicts of Interest

The authors declare no conflicts of interest.

Data Availability Statement

The data that support the findings of this study are available from the corresponding author upon reasonable request.

References

1. K. Geng, T. He, R. Liu, et al., “Covalent Organic Frameworks: Design, Synthesis, and Functions,” *Chemical Review* 120 (2020): 8814–8933.
2. S. Ge, K. Wei, W. Peng, et al., “A Comprehensive Review of Covalent Organic Frameworks (COFs) and Their Derivatives in Environmental Pollution Control,” *Chemical Society Review* 53 (2024): 11259–11302.
3. L. Jiang, Y. Tian, T. Sun, et al., “A Crystalline Polyimide Porous Organic Framework for Selective Adsorption of Acetylene over Ethylene,” *Journal of the American Chemical Society* 140 (2018): 15724–15730.
4. Y. Yusran, B. Miao, S. Qiu, and Q. Fang, “Functional Covalent Organic Frameworks: Design Principles to Potential Applications,” *Accounts of Material Research*, 5 (2024): 1263–1278.
5. C. Ji, C. Kang, B. C. Patra, and D. Zhao, “Flexible Covalent Organic Frameworks: Design, Synthesis, and Applications,” *CCS Chemical*, 6 (2024): 856–881.

6. X. Xu, X. Wu, K. Xu, H. Xu, H. Chen, and N. Huang, "Pore Partition in Two-dimensional Covalent Organic Frameworks," *Nature Communications* 14 (2023): 3360.
7. Z. Mu, Y. Zhu, B. Li, A. Dong, B. Wang, and X. Feng, "Covalent Organic Frameworks with Record Pore Apertures," *Journal of the American Chemical Society* 144 (2022): 5145–5154.
8. F. Chen, H. Zheng, Y. Yusran, H. Li, S. Qiu, and Q. Fang, "Exploring High-connectivity Three-dimensional Covalent Organic Frameworks: Topologies, Structures, and Emerging Applications," *Chemical Society Review* 54 (2025): 484–514.
9. W. Huang, W. Zhang, S. Yang, L. Wang, and G. Yu, "3D Covalent Organic Frameworks from Design, Synthesis to Applications in Optoelectronics," *Small* 20 (2024): 2308019.
10. J. Chang, Z. Zhang, H. Zheng, et al., "Synthesis of three-dimensional covalent organic frameworks through a symmetry reduction strategy," *Nature Chemistry* 17 (2025): 571–581.
11. J.-Y. Weng, M. Yue, Q. Li, et al., "3D interpenetrated Covalent Organic Frameworks," *Coordination Chemistry Reviews* 535 (2025): 216614.
12. S.-Q. Yang, R. Krishna, H. Chen, et al., "Immobilization of the Polar Group into an Ultramicroporous Metal–Organic Framework Enabling Benchmark Inverse Selective CO₂/C₂H₂ Separation with Record C₂H₂ Production," *Journal of the American Chemical Society* 145 (2023): 13901–13911.
13. S. Xian, J. Peng, H. Pandey, et al., "Simultaneous Removal of C₂H₂ and C₂H₆ for C₂H₄ Purification by Robust MOFs Featuring a High Density of Heteroatoms," *Journal of Materials Chemistry A* 11 (2023): 21401–21410.
14. C. Y. Chuah, H. Lee, and T.-H. Bae, "Recent Advances of Nanoporous Adsorbents for Light Hydrocarbon (C₁ – C₃) Separation," *Chemical Engineering Journal* 430 (2022): 132654.
15. Y. Xie, W. Wang, Z. Zhang, et al., "Fine-Tuning the Pore Environment of Ultramicroporous Three-Dimensional Covalent Organic Frameworks for Efficient One-Step Ethylene Purification," *Nature Communication*, 15 (2024): 3008.
16. Z. Zhang, C. Kang, S. B. Peh, et al., "Efficient Adsorption of Acetylene over CO₂ in Bioinspired Covalent Organic Frameworks," *Journal of the American Chemical Society* 144 (2022): 14992–14996.
17. X. Wang, H. Liu, M. Sun, et al., "Functionalization of Covalent Organic Frameworks with Cyclopentadienyl Cobalt for C₂H₂/CO₂ Separation," *Angewandte Chemie International Edition*, 64 (2025): 202420801.
18. Y. Zhou, Y. Xie, X. Liu, et al., "Single-Molecule Traps in Covalent Organic Frameworks for Selective Capture of C₂H₂ from C₂H₄-Rich Gas Mixtures," *Research* 7 (2024): 0458.
19. Y.-X. Ma, Z.-J. Li, L. Wei, S.-Y. Ding, Y.-B. Zhang, and W. Wang, "A Dynamic Three-Dimensional Covalent Organic Framework," *Journal of the American Chemical Society* 139 (2017): 4995–4998.
20. L. Jiang, P. Wang, M. Li, et al., "Construction of a Stable Crystalline Polyimide Porous Organic Framework for C₂H₂/C₂H₄ and CO₂/N₂ Separation," *Chemistry* 25 (2019): 9045–9051.
21. W. Jiang, P. Wang, K.-I. Otake, et al., "Sodium-Ion-Induced Discriminative C₂H₂/CO₂ Adsorption in a Covalent Organic Framework Studied by Solid-State ²³Na NMR," *Journal of Physical Chemistry C* 126 (2022): 15367–15373.
22. F. Yuan, Y. Li, Z. Yuan, et al., "A Grafting Hydrogen-Bonded Organic Framework for Benchmark Selectivity of C₂H₂/CO₂ Separation under Ambient Conditions," *Angewandte Chemie International Edition* 64 (2025): 202414215.
23. F. Xiang, H. Zhang, Y. Yang, et al., "Tetranuclear Cu II Cluster as the Ten Node Building Unit for the Construction of a Metal–Organic Framework for Efficient C₂H₂/CO₂ Separation," *Angewandte Chemie International Edition* 62 (2023): 202300638.
24. Y. Ye, S. Xian, H. Cui, et al., "Metal–Organic Framework Based Hydrogen-Bonding Nanotrap for Efficient Acetylene Storage and Separation," *Journal of the American Chemical Society* 144 (2022): 1681–1689.
25. L. Yang, L. Yan, Y. Wang, et al., "Adsorption Site Selective Occupation Strategy within a Metal–Organic Framework for Highly Efficient Sieving Acetylene from Carbon Dioxide," *Angewandte Chemie International Edition* 133 (2021): 4620–4624.
26. C.-X. Chen, T. Pham, K. Tan, et al., "Regulating C₂H₂/CO₂ Adsorption Selectivity by Electronic-state Manipulation of Iron in Metal-organic Frameworks," *Cell Reports Physical Science* 3 (2022): 100977.
27. N. Kumar, S. Mukherjee, N. C. Harvey-Reid, et al., "Breaking the Trade-off between Selectivity and Adsorption Capacity for Gas Separation," *Chemistry* 7 (2021): 3085–3098.
28. A. Amrein, H. Hollenstein, M. Quack, R. Zenobi, J. Segall, and R. N. Zare, "Fermi Resonance Structure in the CH Vibrational Overtones of CD₃CHO," *Journal of Chemical Physics* 90 (1989): 3944–3951.
29. H. Leclerc, T. Devic, S. Devautour-Vinot, et al., "Influence of the Oxidation State of the Metal Center on the Flexibility and Adsorption Properties of a Porous Metal Organic Framework: MIL-47(V)," *Journal of Physical Chemistry C* 115 (2011): 19828–19840.
30. C. Serre, S. Bourrelly, A. Vimont, et al., "An Explanation for the Very Large Breathing Effect of a Metal–Organic Framework during CO₂ Adsorption," *Advanced Materials* 19 (2007): 2246–2251.
31. I. M. Ibrahim, S. Yunus, and M. A. Hashim, "Relative Performance of Isopropylamine, Pyrrole, and Pyridine as Corrosion Inhibitors for Carbon Steels in Saline Water at Mildly Elevated Temperatures," *International Journal Scientific & Engineering Research* 4 (2013): 2229–2518.
32. R.-B. Lin, L. Li, H. Wu, et al., "Optimized Separation of Acetylene from Carbon Dioxide and Ethylene in a Microporous Material," *Journal of the American Chemical Society* 139 (2017): 8022–8028.
33. L. Zhang, F. Li, J. You, et al., "A Window-Space-Directed Assembly Strategy for the Construction of Supertetrahedron-Based Zeolitic Mesoporous Metal–Organic Frameworks with Ultramicroporous Apertures for Selective Gas Adsorption," *Chemical Science* 12 (2021): 5767–5773.
34. J. Wang, Y. Zhang, Y. Su, et al., "Fine Pore Engineering in a Series of Isoreticular Metal-organic Frameworks for Efficient C₂H₂/CO₂ Separation," *Nature Communications* 13 (2022): 200.

Supporting Information

Additional supporting information can be found online in the Supporting Information section.

Supporting file 1: marc202500317-sup-0001-SupMat.docx